Available online at www.sciencedirect.com
ScienceDirect
International Journal of Heat and Mass Transfer 50 (2007) 4812–4822
International Journal of HEAT and MASS TRANSFER
www.elsevier.com/locate/ijhmt

On the behaviour of hygroscopic wheels: Part I – channel modelling

C.R. Ruivo [a,b,*], J.J. Costa [b], A.R. Figueiredo [b]

[a] Área Departamental de Engenharia Mecânica, Escola Superior de Tecnologia, Universidade do Algarve, Campus da Penha, 8005-139 Faro, Portugal
[b] ADAI, Department of Mechanical Engineering, University of Coimbra, P 3030-788 Coimbra, Portugal

Received 19 January 2006; received in revised form 25 February 2007
Available online 10 May 2007

Abstract

In this paper a detailed mathematical formulation is developed for the numerical modelling of the behaviour of a channel of a hygroscopic compact matrix. A comparison between the detailed version and a simplified one is performed considering a two-dimensional airflow between desiccant parallel plates. The distinct heat and mass transfer phenomena are strongly coupled, and some properties of the airflow and of the desiccant medium exhibit important changes during the sorption processes. Both physical models take into account the gas side and solid side resistances to heat and mass transfer. The wall domain is treated similarly in both models, by taking into account the simultaneous heat and mass transfer together with the water adsorption/desorption process. Two phases co-exist in equilibrium inside the desiccant porous medium, the equilibrium being characterized by sorption isotherms without hysteresis. The detailed model is based on the solution of the differential equations for the conservation of mass, energy and momentum, assuming that no momentum transport exists in the porous wall domain. In the simplified model, the airflow is treated as a bulk flow, the interaction with the wall being evaluated by using appropriated convective coefficients.

Both models are compared in the simulation of a parallel plate channel during an adsorption process. The results show a good agreement for channel lengths greater than 0.1 m. In part II of the paper, the simplified model is adapted to the simulation of the three-dimensional problem in the channel of a hygroscopic rotor, and it is used to perform parametric studies.

Keywords: Adsorption; Desiccant; Hygroscopic rotors; Numerical modelling

1. Introduction

When studying the coupled heat and mass transfer phenomena associated with sorption processes occurring in solid porous media, the first crucial aspect is the characterization of the desiccant material, namely the knowledge of the thermal properties, the diffusion coefficients, the phase equilibrium laws, the hysteresis effects, etc. In this scope, the thesis of Pesaran [1] and Kodama [2] assume a great relevance. In [1], the study of water adsorption in the silica gel particles is focussed on the importance of the internal resistances to mass transfer. The investigation in [2] deals with the experimental characterization of the matrix of a desiccant rotor, made of a composite desiccant medium, a fibrous material impregnated with silica gel.

The experimental and numerical investigation of solid desiccant airflow systems has been the object of numerous fundamental and applied researches (e.g. [1–10]). One such airflow system is the hygroscopic wheel, where the continuous heat and mass exchange between two airflows is promoted by means of a rotary honeycomb matrix. In each channel of the matrix, the important physical phenomena are the heat and mass convection on the gas side of the interface, as well as the heat and mass diffusion and the sorption process in the desiccant wall. The differential equations characterizing the energy and mass conservation laws, as well as the transfer rate equations for mass and energy, have been established for long time, but the

* Corresponding author. Address: Área Departamental de Engenharia Mecânica, Escola Superior de Tecnologia, Universidade do Algarve, Campus da Penha, 8005-139 Faro, Portugal. Tel.: +351 289 800100; fax: +351 289 888405.
E-mail address: cruivo@ualg.pt (C.R. Ruivo).

0017-9310/$ - see front matter © 2007 Elsevier Ltd. All rights reserved.
doi:10.1016/j.ijheatmasstransfer.2007.03.003

Nomenclature

$c^*_{p_f}$	specific heat of the moist air referred to the unit of mass of the mixture
$\bar{c}^*_{p_f}$	mean specific heat of the moist air referred to the unit of mass of the mixture
$\bar{c}^*_{p_{g.v}}$	mean specific heat of the moist air referred to the unit of mass of the mixture
$\bar{c}_{p_{sd}}$	specific heat of the solid desiccant
$\bar{c}_{p_{sub}}$	specific heat of the substrate
$\bar{c}_{p_{wpm}}$	mean specific heat of the wet porous medium
D_f	diffusion coefficient of water vapour in the air
$D_{K,eff}$	effective coefficient of Knudsen diffusion
$D_{m,v}$	diffusion coefficient of water vapour in the air
$D_{m,g}$	diffusion coefficient of air in water vapour
$D_{s,eff}$	effective coefficient of surface diffusion of adsorbed water
d_{hyd}	hydraulic diameter
F_m	mass velocity
H_c	channel half-height (cf. Fig. 3)
H_d	thickness of the desiccant layer
H_p	half-thickness of the channel wall
H_{sub}	half-thickness of the substrate layer
h_{ads}	heat of adsorption
h_{fg0}	latent heat of vaporization at the reference temperature (0 °C)
h_g	enthalpy of air
h_h	convection heat transfer coefficient
h_ℓ	enthalpy of free liquid water
$h^{\cdot}_\ell$	enthalpy of adsorbed water
$h^{\cdot}_{lig}$	heat of wetting
h_m	convection mass transfer coefficient
h_v	enthalpy of vapour
$\dot{J}_{e,gs}$	gas side energy transfer rate at the interface per unit of transfer area
$\dot{J}_{h,gs}$	gas side heat transfer rate at the interface per unit of transfer area
$\dot{J}_{v,gs}$	gas side mass transfer rate at the interface per unit of transfer area
$j_{e,gs}$	gas side convective energy flux at the interface
$j_{h,gs}$	gas side convective heat flux at the interface
$j_{h,ss}$	solid side heat conduction flux at the interface
$j_{\ell,ss}$	solid side surface diffusion flux at the interface
$j_{v,gs}$	gas side convective mass flux at the interface
$j_{v,ss}$	solid side Knudsen diffusion flux at the interface
L_c	channel length
Le	Lewis number
Nu	Nusselt number
p	pressure of the air–vapour mixture
p_{v_s}	saturation pressure
R_g	gas constant of dry air
$R_{g.v}$	gas constant of air–vapour mixture
R_v	gas constant of water vapour
Sh	Sherwood number
S_ϕ	generic source-term in Eqs. (1) and (6)
T	temperature
t	time coordinate
u	x-component of the airflow velocity
u_f	bulk airflow velocity
v	y-component of the airflow velocity
w_v	water vapour content in the moist air
X_ℓ	adsorbed water content (d.b.)
x, y	spatial coordinates

Greek symbols

Γ_ϕ	generic term in Eq. (1)
ε_{dpm}	porosity of the desiccant porous medium
$\varepsilon_{g.v}$	volume fraction of the gaseous mixture within the porous medium
ϕ	generic variable
φ_v	vapour mass fraction in the moist air
κ_ϕ	generic term in Eq. (5) ($\kappa_\phi = 0$ in the wall domain, $\kappa_\phi = 1$ in the airflow domain)
λ	thermal conductivity
$\mu_{g.v}$	dynamic viscosity of the air–vapour mixture
ρ	density
ρ^*	apparent density
ρ_ϕ	generic term in Eq. (5)
ψ	relative pressure, i.e., ratio of the partial to the saturation vapour pressure

Subscripts

f	bulk airflow
g	air
g.v	air–vapour mixture
gs	gas side
i	solid–airflow interface
in	inlet
ini	initial
ℓ	water (free liquid or adsorbed)
out	outlet
sd	solid desiccant
ss	solid side
sub	substrate
v	water vapour
wpm	wet porous medium

complete set of equations has not an analytical solution [11,12]. Methods of solution supported by different simplified treatments of the fluid and the solid domains have been widely used to predict the behaviour of air dehumidifying systems [13–28].

When advanced numerical methods are used to simulate the behaviour of hygroscopic wheels, several critical issues still remain, such as the lack of knowledge of some properties of the porous medium [29–34], the numerical difficulties of handling the coupling between the different phenomena

and the time consumption in the computational calculations [23].

Although it is recognized the importance of validating the numerical results by comparison with experimental data, the bibliographic research shows a lack of information for the complete characterization of the desiccant media as required for the validation of detailed numerical models. In some cases, the degree of accuracy of the measured results is not included and, in other works, a poor degree of accuracy is reported. Moreover, some examples of exhaustive experimental research on the behaviour of a desiccant wheel [35] show significant mass and energy imbalances between the regeneration and the process air streams.

The purpose of the present paper is the numerical modelling of the heat and mass transfer phenomena occurring in hygroscopic rotors. In this part I, a detailed and a simplified model for the parallel plate channel configuration are presented. Simulations are performed to investigate the validity of the simplified model. In part II, given the good agreement of both models in the range of practical interest, the simplified model is adapted to the simulation of the three-dimensional channel of a hygroscopic rotor and is then explored in several parametric studies.

2. Some aspects of the behaviour of hygroscopic rotors

Hygroscopic rotors are dynamic air–air heat and mass exchangers, with relatively low rotation speeds. The matrix of the hygroscopic rotor is a porous medium similar to a honeycomb, mechanically resistant, very compact and with low density, which is cyclically submitted to processes of adsorption and desorption. The most common configuration is schematically illustrated in Fig. 1a, where the adsorption and desorption zones are equal and crossed by counter-current airflows. In Fig. 1b an optimized desiccant wheel with the desorption zone smaller than the adsorption zone is sketched, having a compact corrugated matrix with sinusoidal cross section channels.

The approaching airflow in each zone is generally turbulent. On the other hand, the relatively low values of hydraulic diameter of the channels, frequently less than 5 mm, together with moderate values of the frontal velocity, usually between 1 and 3 m s^{-1}, impose laminar airflow regime inside the channels.

In very short matrixes, the necessary length to stabilize the different boundary layers inside each channel can be significant, particularly for larger hydraulic diameters. In reality, both approaching flows can present instabilities and heterogeneities, which are difficult to be modelled in a rigorous way.

The main applications of hygroscopic rotors are the air dehumidification and the energy recovery in refrigeration or air conditionings installations. The denomination of a hygroscopic rotor depends on the type of application. Enthalpy wheels refer to energy recovery and desiccant wheels to the air dehumidification.

The psychrometric evolutions occurring in the airflows crossing an enthalpy wheel are completely different of those in a desiccant wheel, due to the different inlet conditions of the flows, but mainly to the difference in the rotation speed of the wheel, which is directly related to the cycle duration. The evolutions schematically represented in Figs. 2a and b

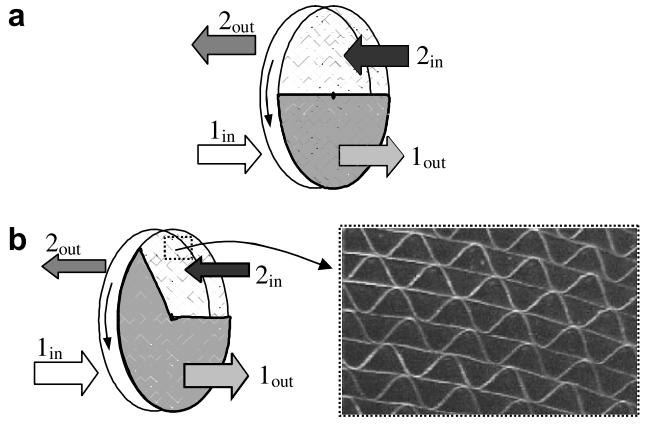

Fig. 1. Hygroscopic rotor: (a) equal adsorption and desorption zones, (b) desorption zone smaller than the adsorption zone (– adsorption zone; – desorption zone).

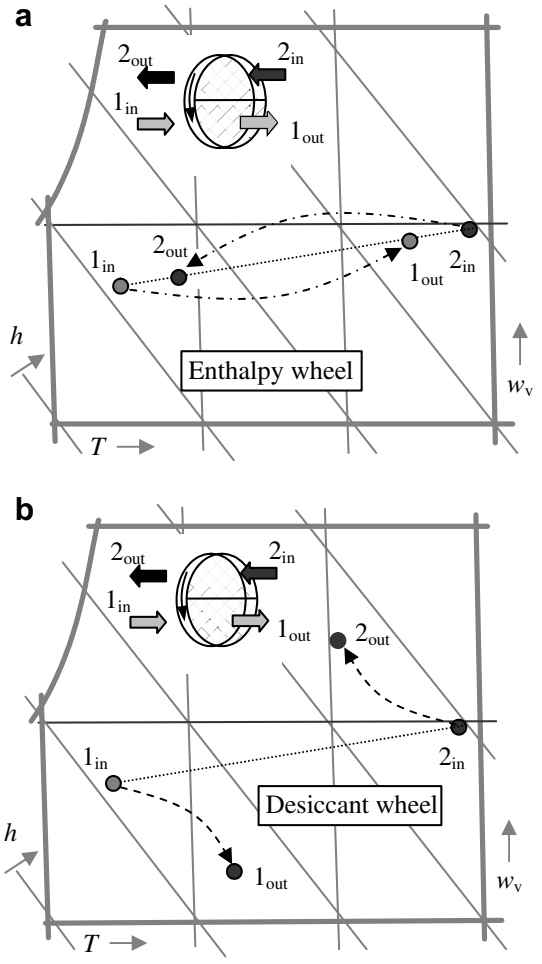

Fig. 2. Psychrometric evolutions in: (a) enthalpy wheel and (b) desiccant wheel.

correspond to optimum rotor behaviours, respectively, for enthalpy and desiccant wheels.

Due to the axial and angular variations during the adsorption/desorption cycle, the matrix exhibits non uniform distributions of adsorbed water content and temperature. The angular gradients depend on the constitution of the wall matrix and also on the rotation speed, being relatively high in desiccant wheels and lower in enthalpy wheels, in which case the rotation speed is significantly higher. In both cases, the radial gradients are usually negligible.

Different definitions for the effectiveness of a hygroscopic rotor can be found in literature. Following the classical analysis of the thermal behaviour of heat exchangers, the concept of effectiveness results from the comparison between the behaviours of the real heat exchanger and an ideal one adopted as a reference. The effectiveness evaluation at steady-state conditions can be performed by experimental techniques or by numerical modelling. The use of the effectiveness method has practical interest, for example in fast energetic analysis of air-conditioning systems, but needs the prior knowledge of the ideal outlet conditions or of the ideal transfer rates. In the case of enthalpy wheels, the ideal behaviour is essentially defined by the inlet conditions of both flows, as illustrated in Fig. 2a. The application of the same procedure to desiccant wheels is not so evident, the solution of the ideal performance being necessarily determined by experiments or by numerical methods. Another important aspect concerns the difficulty to apply the steady-state effectiveness values to desiccant wheels that can exhibit important inertial effects. Moreover, the effectiveness of a hygroscopic rotor depends on both inlet states. Additionally, in the case of desiccant wheels, the use of the effectiveness method appears to be unfeasible because the optimum rotation speed in the ideal process can be, in principle, different from the optimum speed for the real process. In fact, the suitable procedure to evaluate the performance of air conditioning systems that include hygroscopic rotors consists frequently in using the transfer rates given by the rotor manufacturer or those determined by detailed numerical methods.

3. Mathematical and numerical modelling of a channel

The physical domain of the hygroscopic rotor can be considered as a set of small angular slices, the channels in each slice having the same behaviour. The representative channel rotates continuously, and the inlet airflow conditions change, in state and direction, every time the transition between the adsorption and desorption zones occurs. The transient three-dimensional problem is too complex to be solved in a very detailed way, therefore it is necessary to adopt a set of simplifications. For the purpose of comparing the results given by the detailed and the simplified models, the physical domain was taken as a two-dimensional airflow between desiccant parallel plates, under steady-state inlet flow conditions. The hypothesis of two-dimensionality, together with the consideration of cyclic inlet conditions, real wall thickness and ratio of airflow rate to wetted perimeter is frequently adopted when modelling the behaviour of desiccant wheels [25,27], aspects that will be taken into account in part II of this paper. The two-dimensional domain is schematically represented in Fig. 3, where the boundary layers and the profiles of the main variables in both the fluid and the wall domains are also sketched.

The wall domain is modelled in a detailed way, by taking into account the simultaneous heat and mass transfer together with the adsorption/desorption process. Only water adsorption is considered in conjunction with heat and mass diffusion. Two phases co-exist in equilibrium inside the desiccant porous medium, the equilibrium being characterized by sorption isotherms without hysteresis. The properties of the desiccant layer are those of silica–gel RD [1]. The ordinary diffusion of vapour is neglected due to the small dimension of the pores [1]. Therefore, only two mechanisms of mass transport are considered: surface diffusion of adsorbed water and Knudsen diffusion of water vapour.

Two approaches are adopted for the flow domain: a detailed model (MD) that solves the conservation equations of mass, momentum and energy, and a simplified model (MS) that treats the airflow as a bulk flow; the inter-

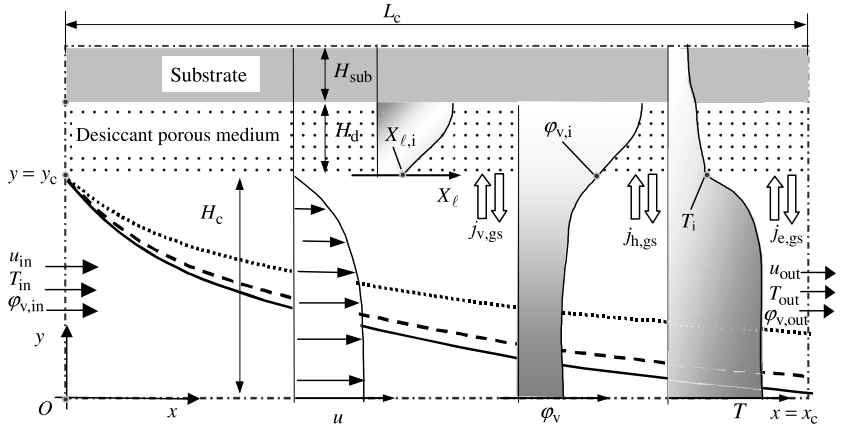

Fig. 3. Schematic representation the boundary layers and the profiles of u, φ_v, X_ℓ and T in a half-channel domain.

face interactions being characterized by the use of convective heat and mass transfer coefficients.

3.1. Conservation equations

The complete set of conservation equations to be solved by the detailed model MD can be reduced to the general form:

$$\frac{\partial}{\partial t}(\rho_\phi \phi) + \frac{\partial}{\partial x_j}\left(\kappa_\phi \rho_\phi u_j \phi - \Gamma_\phi \frac{\partial \phi}{\partial x_j}\right) - S_\phi = 0, \quad (1)$$

where the density ρ_ϕ, the diffusion coefficient Γ_ϕ and the source-term S_ϕ assume the different meanings listed in Table 1, depending on the nature of the generic variable ϕ considered. The different expressions for the source-term are represented in Table 2. The parameter κ_ϕ enables to neutralize the advection term in Eq. (1) for the wall domain. According to this formulation, it is not necessary to solve the mass conservation equation for water vapour inside the porous medium, the mass fraction of vapour being imposed through the local equilibrium condition. Its distribution is used in the evaluation of the local rate of phase change, which corresponds to the source-term $S_{v\ell,d}$ indicated in Table 2.

Table 1
Meaning of ϕ, κ_ϕ, ρ_ϕ, Γ_ϕ, and S_ϕ in generic conservation equation in the detailed model MD

Conservation equation	ϕ	κ_ϕ	ρ_ϕ	Γ_ϕ	S_ϕ
Flow domain					
Mass of the gaseous mixture	1	1	$\rho_{g.v}$	0	0
Mass of water vapour	φ_v	1	$\rho_{g.v}$	$\rho_{g.v} D_{m,v}$	0
Momentum	u_i	1	$\rho_{g.v}$	$\mu_{g.v}$	$S_{u_i,f}$
Energy	T	1	$\rho_{g.v}$	$\lambda_{g.v}/\bar{c}^*_{p_{g.v}}$	$S_{e,f}$
Desiccant domain					
Mass of adsorbed water	X_ℓ	0	ρ^*_{sd}	$\rho^*_{sd} D_{s,eff}$	$S_{v\ell,d}$
Energy	T	0	ρ^*_{sd}	$\lambda_{wpm}/\bar{c}_{p_{wpm}}$	$S_{e,d}$
Substrate domain					
Energy	T	0	ρ_{sub}	$\lambda_{sub}/\bar{c}_{p_{sub}}$	0

Table 2
Source terms in the generic equation of the detailed model MD

Momentum in the flow

$$S_{u_i,f} = \frac{\partial}{\partial x_j}\left(\mu_{g.v}\frac{\partial u_j}{\partial x_i}\right) - \frac{\partial p}{\partial x_i}$$

Energy in the flow

$$S_{e,f} = \frac{\partial}{\partial x_j}\left[D_{m,v}\frac{\partial(\rho_{g.v}\varphi_v)}{\partial x_j}h_v + D_{m,g}\frac{\partial(\rho_{g.v}\varphi_g)}{\partial x_j}h_g - \rho_{g.v}\varphi_v h_{fg0} u_j\right] - \frac{\partial}{\partial t}(\rho_{g.v}\varphi_v h_{fg0})$$

Mass of adsorbed water desiccant layer

$$S_{v\ell,d} = \frac{\partial}{\partial x_j}\left[\frac{D_{K,eff}}{\varepsilon_{g.v}}\frac{\partial(\rho^*_{g.v}\varphi_v)}{\partial x_j}\right] - \frac{\partial(\rho^*_{g.v}\varphi_v)}{\partial t}$$

Energy in the desiccant layer

$$S_{e,d} = \frac{\partial}{\partial t}[-\rho^*_{g.v}\varphi_v h_{fg0} + \rho^*_{sd} X_\ell h^{\cdot}_{lig}] + \frac{\partial}{\partial x_j}\left[\frac{D_{K,eff}}{\varepsilon_{g.v}}\frac{\partial(\rho^*_{g.v}\varphi_v)}{\partial x_j}h_v + D_{s,eff}\rho^*_{sd}\frac{\partial X_\ell}{\partial x_j}h^{\cdot}_\ell\right]$$

The total pressure field in the desiccant porous medium is supposed to be uniform and constant, the density of the gaseous mixture inside the pores and in the airflow being evaluated by:

$$\rho_{g.v} = \frac{p}{R_{g.v}(T + 273.15)}. \quad (2)$$

The apparent density of gaseous mixture inside the pores is evaluated by $\rho^*_{g.v} = \varepsilon_{g.v}\rho_{g.v}$, where the volume fraction of the gaseous mixture inside the porous medium $\varepsilon_{g.v}$ depends on the local content of adsorbed water as:

$$\varepsilon_{g.v} = \varepsilon_{dpm} - X_\ell \rho^*_{sd}/\rho_\ell. \quad (3)$$

The mass fraction of water vapour in the air-mixture inside the desiccant porous medium is evaluated by:

$$\varphi_v = \frac{\psi p_{v_s}}{\psi p_{v_s} + (p - \psi p_{v_s})R_v/R_g}, \quad (4)$$

where p_{v_s} is the saturation pressure and ψ is the ratio of vapour partial pressures p_v/p_{v_s} given by the equilibrium condition in the form of $\psi = f(T, X_\ell)$. The water vapour content in the airflow or inside the pores of the desiccant medium is related with the mass fraction by $w_v = \varphi_v/(1 - \varphi_v)$.

The precedent system of equations for the wall domain is adopted both in the simplified model, MS, and in the detailed one, MD. For the airflow domain, the generic conservation Eq. (1) remains valid for the simplified model MS, provided that $x_j = x$, $u_j = u_f$, $\kappa_\phi = 1$, $\rho_\phi = \rho_f$, $\Gamma_\phi = 0$, and reduces to:

$$\frac{\partial}{\partial t}(\rho_f \phi) + \frac{\partial}{\partial x}(\rho_f u_f \phi) - S_\phi = 0, \quad (5)$$

where the source-term S_ϕ assumes the different meanings indicated in Table 3.

In the model MS, it is assumed that the low mass transfer rate theory is valid [36,37]. The heat convection coefficient h_h is estimated after the Nusselt number for developed laminar channel flow, considering constant and uniform temperature or constant and uniform heat flux at the interface. As for the mass convection coefficient h_m, the Sherwood number is related to Nu according to the Chilton–Colburn analogy:

$$Sh = Nu\, Le^{-1/3}, \quad (6)$$

the Lewis number being defined by

$$Le = \lambda_f/(\rho_f c^*_{p_f} D_f). \quad (7)$$

Thus, the convection coefficients are estimated as

$$h_h = Nu\,\lambda_f/d_{hyd} \quad (8)$$

Table 3
Variable ϕ and source-term S_ϕ in the conservation Eq. (5) for the flow domain in the simplified model MS

Conservation equation	ϕ	S_ϕ
Mass of gaseous mixture	1	$-\frac{h_m\rho_f}{H_c}\frac{\varphi_{v,f}-\varphi_{v,i}}{1-\varphi_{v,i}}$
Mass of water vapour	$\varphi_{v,f}$	$-\frac{h_m\rho_f}{H_c}\frac{\varphi_{v,f}-\varphi_{v,i}}{1-\varphi_{v,i}}$
Energy	T_f	$-\frac{h_m\rho_f}{H_c\bar{c}^*_{p_f}}\frac{\varphi_{v,f}-\varphi_{v,i}}{1-\varphi_{v,i}}(h_{v,i}-h_{fg0})$ $-\frac{h_h}{H_c\bar{c}^*_{p_f}}(T_f-T_i)$
Momentum	u_f	0

and

$$h_m = Sh\,D_f/d_{hyd}. \tag{9}$$

The convective fluxes at the interface are calculated as:

$$j_{v,gs} = h_m\rho_f\frac{\varphi_{v,f}-\varphi_{v,i}}{1-\varphi_{v,i}} \tag{10}$$

and

$$j_{h,gs} = h_h(T_f - T_i), \tag{11}$$

where $\varphi_{v,i}$ and T_i are the instantaneous values at the interface, respectively for the vapour mass fraction and the temperature. In model MD, such fluxes are defined as:

$$j_{v,gs} = \frac{1}{1-\varphi_{v,i}}\left[-D_{m,v}\frac{\partial}{\partial y}(\rho_{g,v}\varphi_v)\right]_{y=y_c^-} \tag{12}$$

and

$$j_{h,gs} = \left[-\lambda_{g,v}\frac{\partial T}{\partial y}\right]_{y=y_c^-}. \tag{13}$$

In both models, the energy flux is evaluated by:

$$j_{e,gs} = j_{h,gs} + j_{v,gs}h_{v,i}, \tag{14}$$

where $h_{v,i}$ is the enthalpy of vapour at the interface.

On the solid side of the interface, the diffusive fluxes are determined in both models by:

$$j_{v,ss} = \left[-\frac{D_{K,eff}}{\varepsilon_{g,v}}\frac{\partial}{\partial y}(\rho^*_{g,v}\varphi_v)\right]_{y=y_c^+}, \tag{15}$$

$$j_{\ell,ss} = \left[-\rho^*_{sd}D_{s,eff}\frac{\partial X_\ell}{\partial y}\right]_{y=y_c^+} \tag{16}$$

and

$$j_{h,ss} = \left[-\lambda_{wpm}\frac{\partial T}{\partial y}\right]_{y=y_c^+}. \tag{17}$$

The local mass and energy balances at the interface lead to the following relations:

$$j_{v,gs} = j_{v,ss} + j_{\ell,ss} \tag{18}$$

and

$$j_{v,gs}h_{v,i} + j_{h,gs} = j_{v,ss}h_{v,i} + j_{\ell,ss}h_{\ell,i} + j_{h,ss}. \tag{19}$$

The energy balance can also be written as:

$$(j_{h,gs} - j_{h,ss}) + j_{\ell,ss}h_{ads,i} = 0. \tag{20}$$

3.2. Initial and boundary conditions

In this part I of the paper, a comparison is made of the results obtained with both MD and MS models when modelling the same adsorption process. The set of conditions used with the detailed model MD are:

(I) *Initial conditions*. Uniform distributions of T and X_ℓ are imposed in the desiccant medium. The same temperature distribution is assigned to the substrate. The airflow domain is assumed to be initially in thermodynamic equilibrium with the desiccant medium. The calculation of the airflow field starts with a parabolic velocity distribution.

(II) *Inlet airflow condition*. Uniform and constant distributions of $u = u_{in}$ (or the corresponding mass velocity, $F_m = F_{m,in}$), T, φ_v and $\rho_{g,v}$ are imposed.

(III) *Outlet airflow condition*. Zero normal gradients are specified to all variables at the outlet section, except for u which is iteratively specified to ensure overall mass balance following a multiplicative correction procedure as described in Costa et al. [38].

(V) *Interface conditions*. At the solid–gas interface, the no-slip condition is assumed for the velocity and the continuity of mass and the energy transport is ensured by the balances expressed by Eqs. (18) and (19), respectively. The desiccant–substrate interface is impermeable to the mass transport.

(VI) *Symmetry condition*. The upper and lower boundaries of the calculation domain are coincident with planes of geometric and physical symmetry. Therefore, a zero normal gradient condition is applied to neutralize any transport phenomena. Both ends of the wall are assumed impermeable and adiabatic.

Concerning the model MS, the boundary conditions are different only at the solid–gas interface, where the mass and heat fluxes are estimated through Eqs. (10) and (11), respectively.

3.3. Numerical solution procedure

In both models MD and MS, the partial differential equations were discretized using the finite volume method. The advection terms in the conservation equations are discretized via the hybrid central-upwind differencing scheme,

Table 4
Parameters of dry silica gel RD [1]

Apparent density	$\rho^*_{sd} = 1129\ \mathrm{kg\ m^{-3}}$
Porosity	$\varepsilon^*_{dpm} = 0.485$
Thermal conductivity	$\lambda_{sd} = 0.144\ \mathrm{W\ m^{-1}\ °C^{-1}}$
Specific heat	$\bar{c}_{p_{sd}} = 921\ \mathrm{J\ kg^{-1}\ °C^{-1}}$

Table 5
Parameters related to the adsorption (derived from Pesaran [1]): X_ℓ in ($\mathrm{kg\ kg^{-1}}$) and T in (°C)

Equilibrium condition

$$\psi = 1.0132 - \sqrt{1.0265 + 2.632X_\ell} \text{ or } X_\ell = 0.77\psi - 0.38\psi^2$$

Heat of wetting ($\mathrm{J\ kg^{-1}}$)

$$h^*_{lig} = 1000 \times (-375.867 - 550\log X_\ell + 420X_\ell)$$

Adsorbed water enthalpy ($\mathrm{J\ kg^{-1}}$)

$$h^*_\ell = 5 \times 10^{-6}T^4 + 0.0027T^3 - 0.4278T^2 + 4201.7T - 1000 \times (420X_\ell - 375.867 - 550\log X_\ell)$$

Adsorption heat ($\mathrm{J\ kg^{-1}}$)

$$h_{ads} = -0.02T^3 + T^2 - 2386.2T + 2501600 + 1000 \times (420X_\ell - 375.867 - 550\log X_\ell)$$

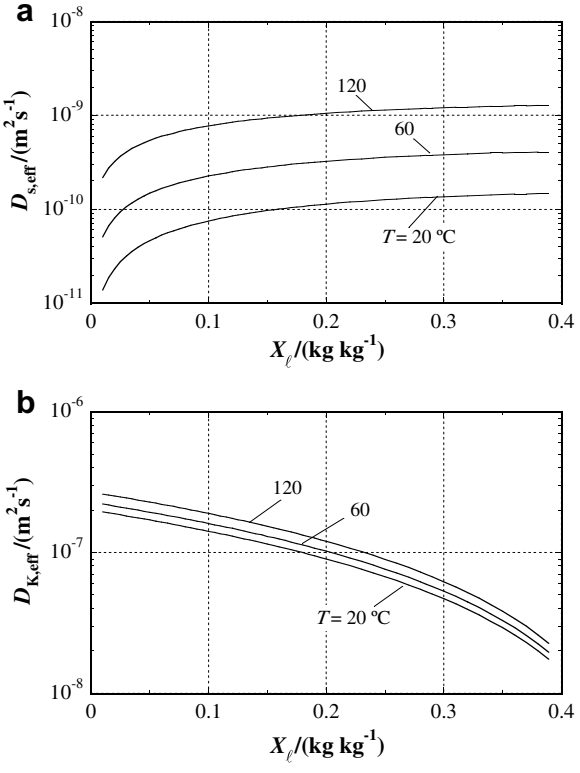

Fig. 4. Effective coefficients for: (a) surface diffusion and (b) Knudsen diffusion (derived from Pesaran [1]).

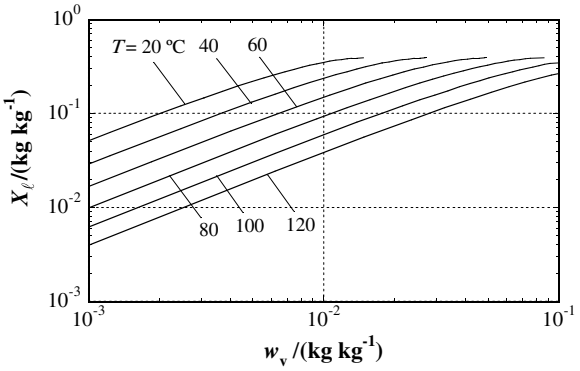

Fig. 5. Hygrothermal equilibrium for the pair water–silica gel RD (relations derived in [40] after the expressions of Pesaran [1]).

Table 6
Initial and inlet flow conditions for the adsorption process

Initial temperature	$T_{ini} = 100$ °C
Initial pressure	$p_{ini} = 101\,325$ Pa
Initial adsorbed water content	$X_{\ell,ini} = 0.012\ \mathrm{kg\ kg^{-1}}$
Inlet temperature	$T_{in} = 30$ °C
Inlet water vapour content	$w_{v,in} = 0.01\ \mathrm{kg\ kg^{-1}}$
Inlet mass velocity	$F_{m,in} = 1.5\ \mathrm{kg\ s^{-1}\ m^{-2}}$

and the SIMPLEC algorithm is used to iteratively calculate the velocity and pressure fields. The values of the diffusion coefficients at the control–volume interfaces are estimated by the harmonic mean, thus allowing the conjugate and simultaneous solution in both gas and solid domains (cf. Patankar [39]). Preliminary grid-independence tests were carried out to choose a numerical grid with a suitable refinement near the interface [40].

The system of equations could be solved separately for each sub-domain (airflow, desiccant and substrate domains). In the present work, however, the energy and the vapour mass transport equations are solved in a conjugate procedure that covers simultaneously all sub-domains, without using the above described interface conditions. Within the desiccant sub-domain, the equilibrium value of the vapour mass fraction given by Eq. (4) is locally specified, according to the procedure suggested in Patankar [39].

3.4. Parameters for global behaviour analysis

To characterize the global behaviour of the channel, a set of parameters is defined below. The mass, heat and energy transfer rates, per unit of transfer area, are evaluated respectively by:

$$\dot{J}_{v,gs} = \frac{1}{x_c}\int_0^{x_c} j_{v,gs}\mathrm{d}x, \tag{21}$$

$$\dot{J}_{h,gs} = \frac{1}{x_c}\int_0^{x_c} j_{h,gs}\mathrm{d}x \tag{22}$$

and

$$\dot{J}_{e,gs} = \frac{1}{x_c}\int_0^{x_c} j_{e,gs}\mathrm{d}x. \tag{23}$$

The outlet bulk airflow values of temperature, mass fraction, water vapour content and density are estimated in the model MD by, respectively:

$$T_{out} = \frac{\int_0^{y_c} \rho_{g.v}\bar{c}^*_{p_{g.v}} uT\Big|_{x=x_c}\mathrm{d}y}{\int_0^{y_c} \rho_{g.v}\bar{c}^*_{p_{g.v}} u\Big|_{x=x_c}\mathrm{d}y}, \tag{24}$$

$$\varphi_{v,out} = \frac{\int_0^{y_c} \rho_{g.v} u\varphi_v|_{x=x_c}\mathrm{d}y}{\int_0^{y_c} \rho_{g.v} u|_{x=x_c}\mathrm{d}y}. \tag{25}$$

$$w_{v,out} = \frac{\int_0^{y_c} \rho_{g.v} u\varphi_v|_{x=x_c}\mathrm{d}y}{\int_0^{y_c} (1-\varphi_v)\rho_{g.v} u|_{x=x_c}\mathrm{d}y}. \tag{26}$$

and

$$\rho_{f,out} = \frac{\int_0^{y_c} \rho_{g.v} u|_{x=x_c}\mathrm{d}y}{\int_0^{y_c} u|_{x=x_c}\mathrm{d}y}, \tag{27}$$

the outlet bulk airflow velocity being given by:

$$u_{out} = \frac{1}{\rho_{f,out} y_c}\int_0^{y_c} \rho_{g.v} u|_{x=x_c}\mathrm{d}y. \tag{28}$$

3.5. Evaluation of properties and coefficients

Both models take into account the changes occurring in properties and diffusion coefficients in both the airflow and the desiccant domains. The major part of the relations for the dry air, water vapour and liquid water was derived from thermodynamics tables [41] in the form of polynomial expressions [40]. The properties of the air-mixture such as $\bar{c}^*_{p_{g.v}}$, $\bar{c}^*_{p_f}$, $c^*_{p_f}$, $\lambda_{g.v}$, λ_f and $\mu_{g.v}$ are weighted averages based on the dry air and water vapour mass fractions. Similarly, the properties $\bar{c}_{p_{wpm}}$ and λ_{wpm} of the wet desiccant medium are weighted averages based on the mass fraction of each component (dry-air, water vapour, adsorbed water and dry desiccant). Some properties of the desiccant medium

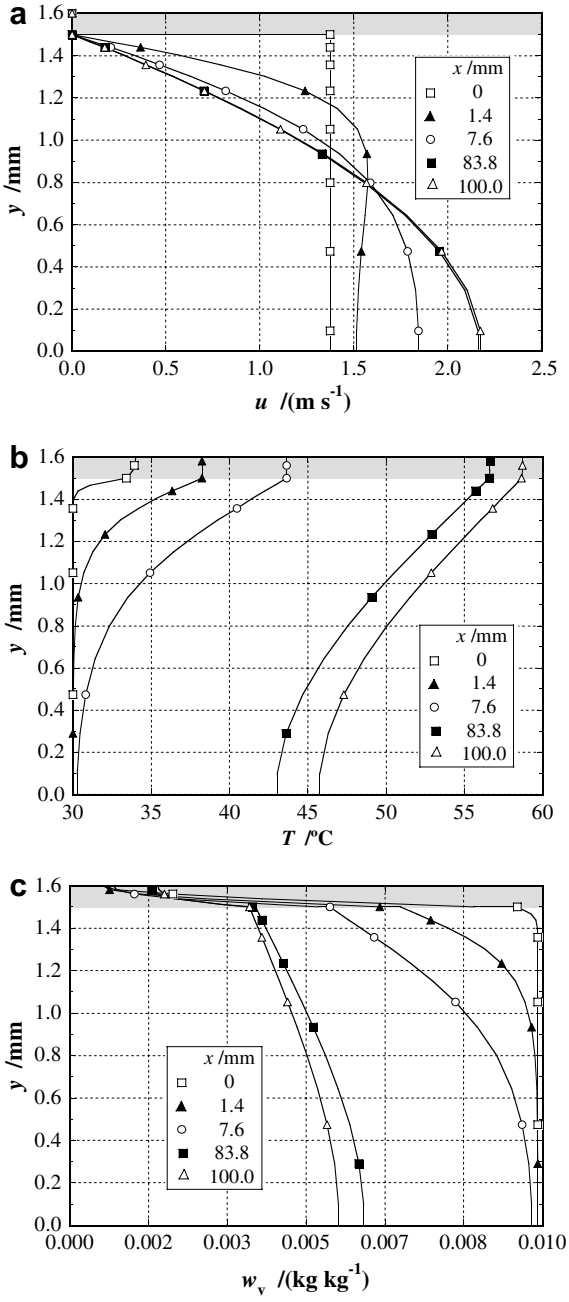

Fig. 6. Profiles of (a) u velocity, (b) temperature and (c) water vapour content. ($L_c = 0.1$ m, $t = 10$ s).

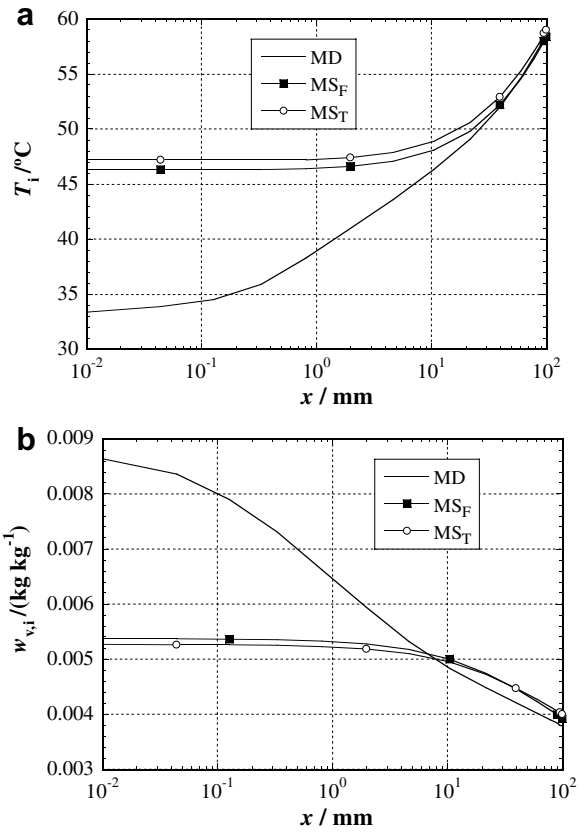

Fig. 7. State of the interface: (a) temperature and (b) water vapour content ($L_c = 0.1$ m, $t = 10$ s).

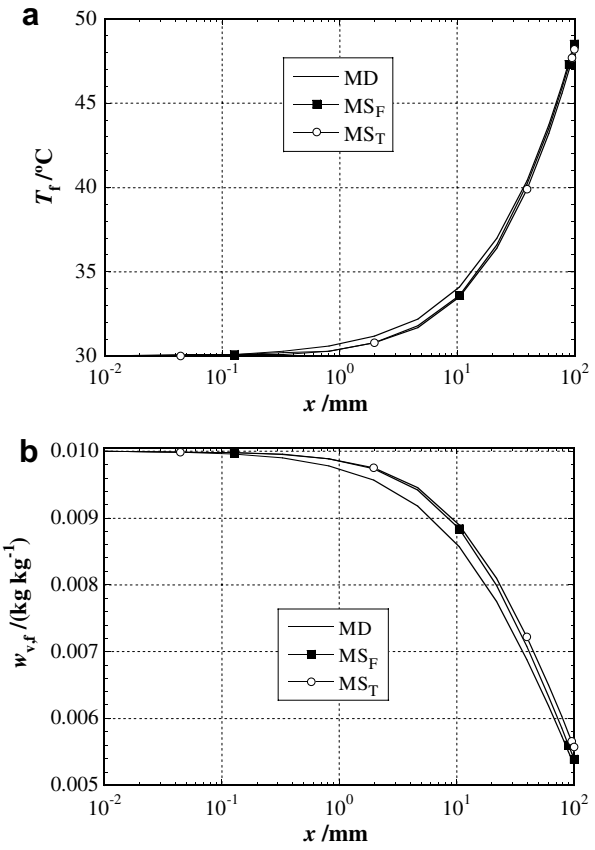

Fig. 8. State of the bulk flow: (a) temperature and (b) water vapour content.

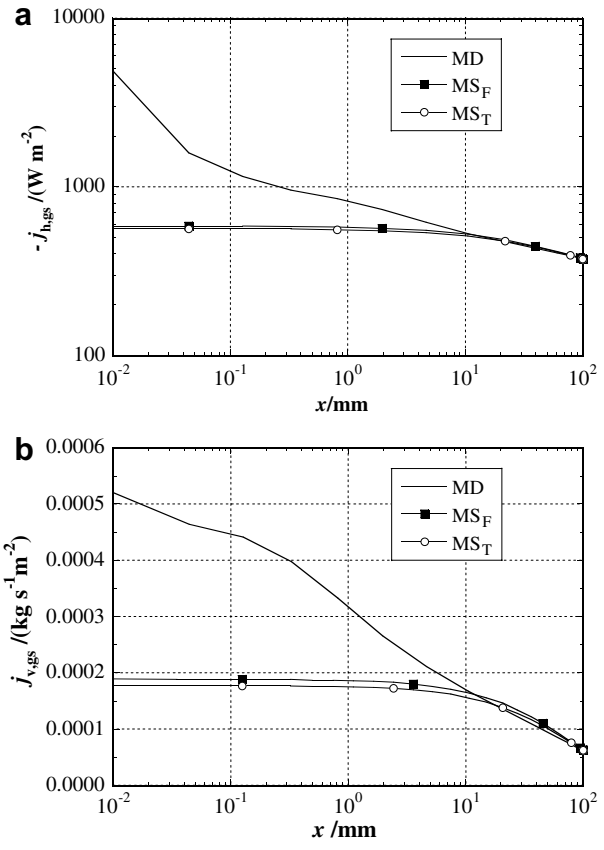

Fig. 9. Heat (a) and mass (b) convective fluxes along the interface.

are listed in Table 4. The equilibrium condition, the heat of wetting, the adsorbed water enthalpy and the adsorption heat were estimated using the relations for silica gel indicated in Table 5.

The strong dependence of the mass diffusion coefficients in the desiccant medium on the temperature and the adsorbed water content is considered in the numerical modelling, and it is illustrated in Figs. 4a and b. The equilibrium condition for the pair water–silica gel RD used in the models is plotted in Fig. 5, in the form $X_\ell = f(w_v, T)$. The empirical relations used for both Figs. 4 and 5 are presented in Ruivo [40] and were derived after the expressions in Pesaran [1] for silica–gel RD.

4. Comparative analysis between the detailed and the simplified models

Calculations were made with both the reference model MD and the simplified model MS to simulate the adsorption process in a static channel. Two versions of the simplified model, named MS_F and MS_T, were used considering fully developed laminar flow between two parallel plates and the values $Nu_F = 8.23$ and $Nu_T = 7.54$, as provided in [41] for the boundary conditions of, respectively, uniform and constant heat flux and of uniform and constant wall temperature.

Several cases with different channel length values from 0.01 to 0.5 m were considered. The half-height of the channel H_c and the wall half-thickness H_p were fixed at 1.5 mm and 0.1 mm, respectively. The initial and the inlet flow conditions are listed in Table 6. The wall was supposed to be formed only by desiccant, i.e., $H_p = H_d$.

The first set of results concerns the transient response of a channel with $L_c = 0.1$ m. Figs. 6a–c illustrate the profiles predicted by the model MD at $t = 10$ s for u, T and w_v, respectively, in five different cross sections. It is seen that the flow achieves the full dynamic development inside the channel, but the thermal and the mass boundary layers are still developing at $x = L_c$.

The results obtained with both models MD and MS are compared in Figs. 7–9: the longitudinal variations of temperature and water vapour content at the interface in Fig. 7, the state of the bulk flow along the channel in Fig. 8, and the convective fluxes in Fig. 9. From the analysis of this set of figures, it may be concluded that, except for a very short entrance region ($x < 10$ mm), a good agreement exists between the detailed and simplified models.

Figs. 10a–d show the time evolutions of the mass transfer rate per unit of transfer area for distinct channels lengths from 0.01 to 0.5 m. The results evidence a very good agreement between both MD and MS models for $L_c \geqslant 0.1$ m, thus justifying the use of the simplified model for the simulation of hygroscopic rotors, of which the

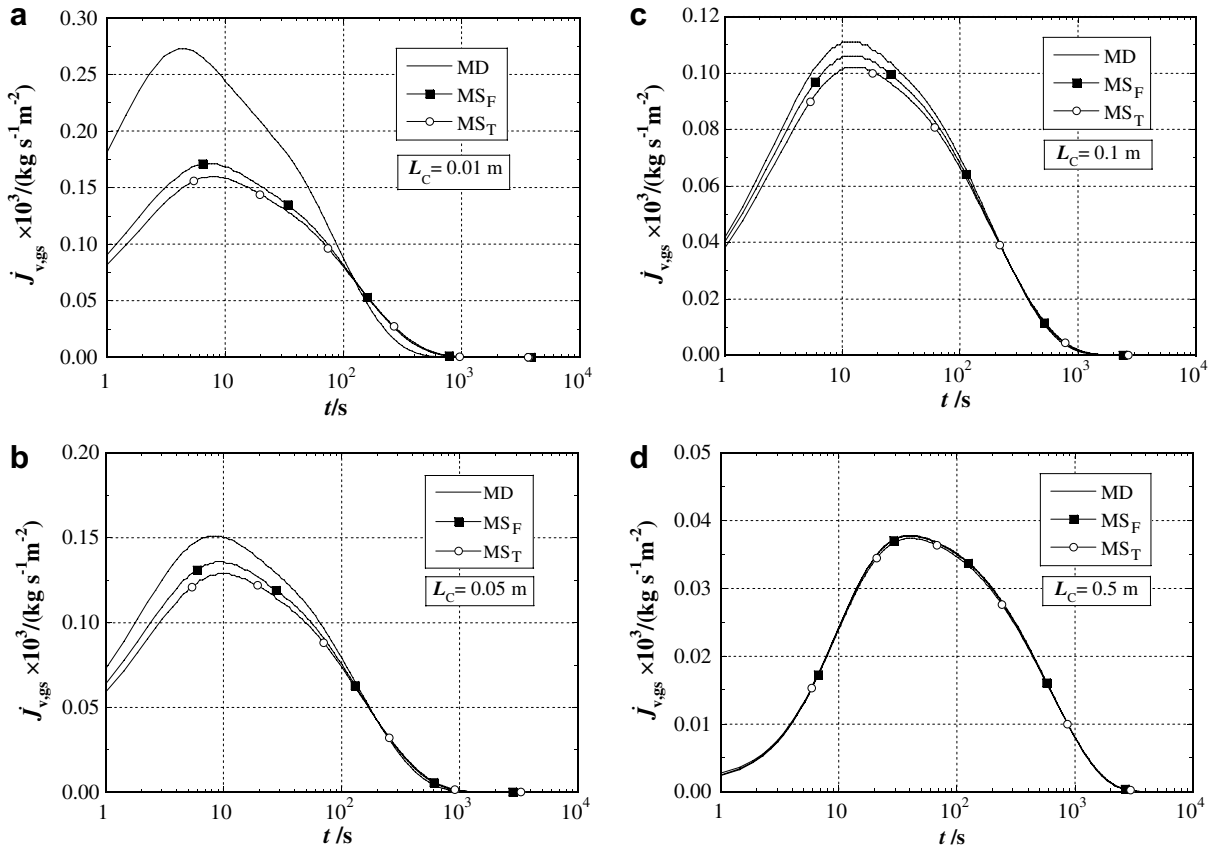

Fig. 10. Time evolutions of the mass transfer rate per unit of transfer area, for different channel lengths: (a) $L_c = 0.01$ m; (b) $L_c = 0.05$ m; (c) $L_c = 0.1$ m and (d) $L_c = 0.5$ m.

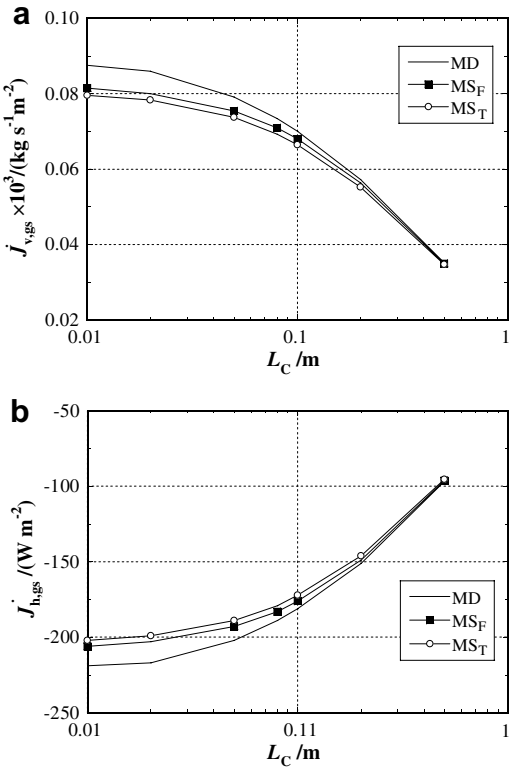

Fig. 11. Convective (a) mass and (b) heat transfer rates per unit of transfer area at $t = 100$ s.

channels in practice are usually longer than 100 mm. This conclusion is corroborated by Figs. 11a and b, where the dependence of the convective mass and heat transfer rates on the channel length is evidenced, for a particular moment of the adsorption process.

5. Conclusions

Detailed and simplified models were formulated enabling the numerical prediction of the heat and mass transfer occurring in a two-dimensional channel configuration of parallel plane walls.

The wall domain is treated in detail in both models, considering the internal time-varying fields of variables like the water vapour mass fraction, the diffusion coefficients, the Knudsen diffusion and surface diffusion fluxes, the thermal fluxes, as well as the phase change in the desiccant layer. In the airflow domain, the hypothesis of bulk flow is adopted in the simplified model concerning the estimation of the convective mass and heat transfer coefficients, and the conservation equations are solved as one-dimensional. In the detailed model, the airflow field is obtained after the solution of the two-dimensional conservation equations for the momentum, mass and energy, the latter being solved in a conjugate procedure.

Both models were used to simulate the channel behaviour in an adsorption process, considering different lengths

from 0.01 to 0.5 m. A comparative analysis showed a very good agreement for channel lengths greater than 0.1 m, which means that the entrance region effects are negligible when $L_c/H_c > 67$. This encourages the use of the simplified model for the simulation of real hygroscopic rotors, which matrices present in general values of the ratio L_c/H_c greater than 67.

References

[1] A. Pesaran, Moisture transport in silica gel particle beds, PhD thesis, University of California, Los Angels, 1983.

[2] A. Kodama, Experimental study on optimization of a honeycomb rotor continuous adsorber operated with thermal swing, PhD thesis, Faculty of Engineering, Kumamoto University, Japan, 1996.

[3] R.B. Holmberg, Combined heat and mass transfer in regenerators with hygroscopic materials, ASME J. Heat Transfer 101 (1979) 205–210.

[4] E. Van Den Bulk, J.W. Mitchell, S.A. Klein, The use of dehumidifiers in desiccant cooling and dehumidification systems, ASME J. Heat Transfer 108 (3) (1986) 684–692.

[5] J.Y. San, Heat and mass transfer in a two-dimensional cross-flow regenerator with a solid heat conduction effect, Int. J. Heat Mass Transfer 36 (3) (1993) 633–643.

[6] W. Zheng, W.M. Worek, D. Novosel, Performance optimization of rotary dehumidifiers, ASME J. Sol. Energ. Eng. 117 (1) (1995) 40–44.

[7] Y. Fujii, N. Lior, Conjugate heat and mass transfer in a desiccant airflow system: a numerical solution method, Numer. Heat Transfer Part A 29 (7) (1996) 689–706.

[8] C.J. Simonson, R.W. Besant, Heat and moisture transfer in desiccant coated rotary energy exchangers: part I. Numerical model, Int. J. Heating, Ventilating, Air-Conditioning Refrigerating Res. 3 (4) (1997) 325–350.

[9] C.J. Simonson, R.W. Besant, Energy wheel effectiveness: part I – development of dimensionless groups, Int. J. Heat Mass Transfer 42 (12) (1999) 2161–2170.

[10] J.W. Jeong, S.A. Mumma, Practical thermal performance correlations for molecular sieve and silica gel loaded enthalpy wheels, Appl. Therm. Eng. 25 (5–6) (2005) 719–740.

[11] D. Charoensupaya, W.M. Worek, Effects of adsorbent heat and mass transfer resistances on the performance of an open-cycle adiabatic desiccant cooling system, Heat Recov. Syst. CHP 8 (6) (1988) 537–548.

[12] P. Majumdar, Heat and mass transfer in composite pore structures for dehumidification, Sol. Energy 62 (1) (1998) 1–10.

[13] I.L. Maclaine-Cross, P.J. Banks, Coupled heat and mass transfer in regenerators-prediction using an analogy with heat transfer, Int. J. Heat Mass Transfer 15 (6) (1972) 1225–1242.

[14] P.J. Banks, Coupled equilibrium heat and single adsorbate transfer in fluid flow through a porous medium – I. Characteristic potentials and specific capacity ratios, Chem. Eng. Sci. 27 (5) (1972) 1143–1155.

[15] H. Ghezelayagh, D. Gidaspow, Micro-macropore model for sorption of water on silica gel in a dehumidifier, Chem. Eng. Sci. 37 (8) (1982) 1181–1197.

[16] E. Van Den Bulk, J.W. Mitchell, S.A. Klein, Design theory for rotary heat and mass exchangers – I. Wave analysis of rotary heat and mass exchangers with infinite transfer coefficients, Int. J. Heat Mass Transfer 28 (8) (1985) 1575–1586.

[17] E. Van Den Bulk, J.W. Mitchell, S.A. Klein, Design theory for rotary heat and mass exchangers – II. Effectiveness-number-of-transfer-units method for rotary heat and mass exchangers, Int. J. Heat Mass Transfer 28 (8) (1985) 1587–1595.

[18] A.A. Pesaran, A. Mills, Moisture transport in silica gel packed beds – I. Theoretical study, Int. J. Heat Mass Transfer 30 (6) (1987) 1037–1049.

[19] P. Majumdar, W.M. Worek, Performance of an open-cycle desiccant cooling system using advanced desiccant matrices, Heat Recov. Syst. CHP 9 (4) (1989) 299–311.

[20] P. Majumdar, W.M. Worek, Combined heat and mass transfer in a porous adsorbent, Energy 14 (3) (1989) 161–175.

[21] W. Zheng, W.M. Worek, Numerical simulation of combined heat and mass transfer processes in a rotary dehumidifier, Numer. Heat Transfer Part A 23 (2) (1993) 211–232.

[22] J.Y. San, S.C. Hsiau, Effect of axial solid heat conduction and mass diffusion in a rotary heat and mass regenerator, Int. J. Heat Mass Transfer 36 (8) (1993) 2051–2059.

[23] E.E. Chant, S.M. Jeter, On the use of the parabolic concentration profile assumption for a rotary desiccant dehumidifier, ASME J. Sol. Energ. Eng. 117 (1) (1995) 317–322.

[24] C.C. Ni, J.Y. San, Mass diffusion in a spherical microporous particle with thermal effect and gas-side mass transfer resistance, Int. J. Heat Mass Transfer 43 (12) (2000) 2129–2139.

[25] Y.J. Dai, R.Z. Wang, H.F. Zhang, Parameter analysis to improve rotary desiccant dehumidification using a mathematical model, Int. J. Therm. Sci. 40 (4) (2001) 400–408.

[26] C.R. Ruivo, A.R. Figueiredo, J.J. Costa, Simplified simulation of the heat and mass transfer in a desiccant medium used in desiccant-evaporative cooling system, HPC'01, in: Proceedings of the Second International Heat Powered Cycles Conference, Paris, France, 2001, pp. 473–478.

[27] X.J. Zhang, Y.J. Dai, R.Z. Wang, A simulation study of heat and mass transfer in a honeycomb rotary desiccant dehumidifier, Appl. Therm. Eng. 23 (8) (2003) 989–1003.

[28] M.N. Golubovic, W.M. Worek, Influence of elevated pressure on sorption in desiccant wheels, Numer. Heat Transfer Part A 45 (9) (2004) 869–886.

[29] A.A. Pesaran, A. Mills, Moisture transport in silica gel packed beds – II. Experimental study, Int. J. Heat Mass Transfer 30 (6) (1987) 1051–1060.

[30] M. Beccali, F. Butera, R. Guanella, R.S. Adhikari, Simplified models for the performance evaluation of desiccant wheel dehumidification, Int. J. Energ. Res. 27 (1) (2003) 17–29.

[31] R.K. Collier, Desiccant properties and their effect in cooling system performance, ASHRAE Trans. 95 (1) (1989) 823–827.

[32] T. Lindholm, Desiccant cooling – a literature survey, D49:2000, Department of Building Services Engineering, Chalmers University of Technology, Goteborg, 2000.

[33] H.I. Henderson, J.R. Sand, An hourly building simulation tool to evaluate hybrid desiccant system configuration options, ASHRAE Trans. 109 (2) (2003) 551–564.

[34] L.A. Sphaier, W.M. Worek, Analysis of heat and mass transfer in porous sorbents used in rotary regenerators, Int. J. Heat Mass Transfer 47 (14–16) (2004) 3415–3430.

[35] J.M. Cejudo, R. Moreno, A. Carrillo, Physical and neural network models of a silica–gel desiccant wheel, Energ. Buildings 34 (8) (2002) 837–844.

[36] R.B. Bird, W.E. Stewart, E.N. Lighfoot, Transfer Phenomena, John Wiley & Sons, Inc, 1960.

[37] A.F. Mills, Heat and Mass Transfer, Irwin, 1985.

[38] J.J. Costa, L.A. Oliveira, D. Blay, Test of several versions of the k–ϵ turbulence modelling of internal mixed convection flows, Int. J. Heat Mass Transfer 42 (23) (1999) 803–819.

[39] S.V. Patankar, Numerical Heat Transfer and Fluid Flow, Hemisphere, McGraw-Hill, Washington, DC, 1980.

[40] C.R. Ruivo, Modelação numérica dos fenómenos de trasnferência de calor e de massa em rodas higroscópicas, PhD thesis, University of Coimbra, Coimbra, Portugal, 2005.

[41] Y. Çengel, Heat Transfer – A Practical Approach, McGraw-Hill, 1998.